ACS ES&T Engineering

pubs.acs.org/estengg

Article

Evaluation of a Porous Membrane as a Mass-Transfer Efficient Structure for the Adsorption of Per- and Polyfluoroalkyl Substances from Drinking Water

Jeein Kim, Liliya Chernysheva, Jialing Xu, Matthew McClure, David R. Latulippe, William A. Phillip, and Kyle Doudrick*

Cite This: *ACS EST Engg.* 2024, 4, 995−1006

Read Online

ACCESS | Metrics & More | Article Recommendations | Supporting Information

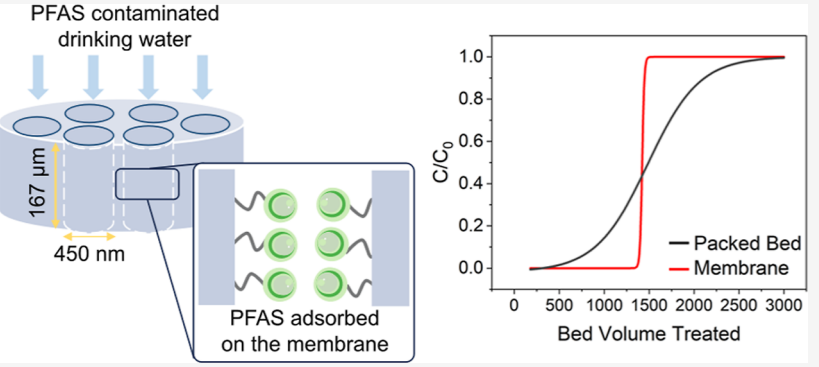

ABSTRACT: With drinking water regulations forthcoming for per- and polyfluoroalkyl substances (PFAS), the need for cost-effective treatment technologies has become urgent. Adsorption is a key process for removing or concentrating PFAS from water; however, conventional adsorbents operated in packed beds suffer from mass transfer limitations. The objective of this study was to assess the mass transfer performance of a porous polyamide adsorptive membrane for removing PFAS from drinking water under varying conditions. We conducted batch equilibrium and dynamic adsorption experiments for perfluorooctanesulfonic acid, perfluorooctanoic acid, perfluorobutanesulfonic acid, and undecafluoro-2-methyl-3-oxahexanoic acid (i.e., GenX). We assessed various operating and water quality parameters, including flow rate (pore velocity), pH, ionic strength (IS), and presence of dissolved organic carbon. Outcomes revealed that the porous adsorptive membrane was a mass transfer-efficient platform capable of achieving dynamic capacities similar to equilibrium capacities at fast interstitial velocities. The adsorption mechanism of PFAS to the membrane was a mixture of electrostatic and hydrophobic interactions, with pH and IS controlling which interaction was dominant. The adsorption capacity of the membrane was limited by its surface area, but its site density was approximately five times higher than that of granular activated carbon. With advances in molecular engineering to increase the capacity, porous adsorptive membranes are well suited as alternative adsorbent platforms for removing PFAS from drinking water.

KEYWORDS: *PFAS, adsorption, polyamide membrane, dynamic capacity, mass transfer*

1. INTRODUCTION

Per- and polyfluoroalkyl substances (PFAS) are persistent synthetic organic contaminants (number of PFAS > 9,000[1]) that are ubiquitous in the environment and pose an emerging threat to human and ecological health.[2−15] PFAS have been detected in numerous drinking water sources and in treated drinking water across the United States.[14,16,17] In 2023, the Environmental Protection Agency (EPA) proposed a maximum contaminants level of 4 ng L^{-1} for perfluorooctanoic acid (PFOA) and perfluorooctanesulfonic acid (PFOS), and a combined hazard index of 1.0 for perfluorononanoic acid (PFNA), perfluorohexanesulfonic acid (PFHxS), perfluorobutanesulfonic acid (PFBS), and hexafluoropropylene oxide (HFPO-DA or GenX), with health-based values of 10, 9, 2000, and 10 ppt, respectively.[18] Implementing these limits is expected to result in significant capital and operating costs. For example, the EPA predicts that a 10 MGD plant using a granular activated carbon (GAC) treatment system would require a capital investment of $7 million, with annual operation and maintenance costs of $10 million.[18]

Received: October 27, 2023
Revised: March 24, 2024
Accepted: March 26, 2024
Published: April 11, 2024

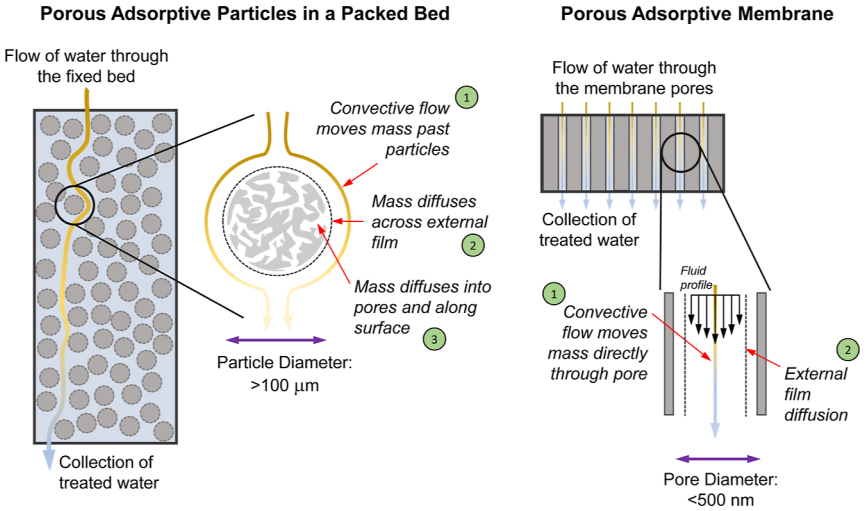

Figure 1. Schematic detailing mass transfer (left) in a packed bed filled with porous adsorptive particles and (right) in a porous adsorptive membrane.

Conventional drinking water treatment technology often fails to adequately remove PFAS. A global survey of 447 finished tap water samples found that the average concentrations of PFOA and PFOS were 4.4 and 8.1 ng L^{-1}, respectively, exceeding the proposed standards of 4 ng L^{-1}.[17] Even bottled water, which undergoes more advanced treatment processes such as reverse osmosis, contained 32 PFAS with concentrations ranging from 0.17 to 18.9 ng L^{-1}.[17] The widespread occurrence of PFAS at concentrations above the EPA's proposed drinking water standards highlights the pressing need to develop cost-effective and efficient technologies for drinking water treatment.

Adsorption processes remain a cost-effective treatment option for removing PFAS from drinking water. Extensive research has been conducted on the use of adsorbents to remove PFAS from water.[19−37] Commercial adsorbents are typically porous receiving media (e.g., GAC, ion exchange [IX] resins) that are packed in a fixed bed to maximize the active surface-area-to-volume ratio to provide a high adsorption capacity.[37−39] This packed bed approach is hampered by significant mass transfer limitations and flow channeling. For binding to occur with adsorptive processes, target solutes must transfer from the bulk solution to active sites on the surface or within the pore structure of the adsorbent. Figure 1 depicts a schematic that details the mass transfer processes of a packed bed in comparison with that of a porous adsorptive membrane platform investigated herein. In a packed bed, the solute mass is driven by convection through the pore space of the bed and to the adsorbent surface. (1) Convective flow causes a hydrodynamic boundary layer (or film) to form around the adsorbent, which in turn creates a concentration boundary layer. (2) When the solute mass reaches the boundary layer, it must diffuse through the film, called external film diffusion. The solute mass then diffuses into the pores until it reaches an adsorption site either through (3) pore diffusion or (4) surface diffusion. The pore/surface diffusion mass transfer processes are commonly the slowest, or rate-determining step. For porous particulates, the characteristic dimension that the solute must diffuse to reach an adsorption site is proportional to the size of the adsorbent. This dimension is typically greater than 100 μm, and since pore/surface diffusion is the slowest rate, these long transport lengths into the bulk of the adsorbent leads to poor adsorption performance. Moreover, the random packing of the adsorbents in the fixed bed produces flow channels with a broad distribution of sizes. Here, contaminated fluid in the larger channels can bypass the active adsorbent surfaces, further hampering performance. Overall, the diffusive mass transfer limitation of fixed beds and flow channeling are major drawbacks that lead to poor adsorption efficiencies and necessitate long contact times that ultimately increase operating costs.

Porous adsorptive membranes are an emerging platform that can potentially overcome the mass transfer limitations hindering conventional particulate adsorbents. A schematic of the mass transfer process in the porous adsorptive membrane is depicted in Figure 1. In contrast to packed beds, the solute mass in the adsorptive membrane is transferred by convection directly through the pores containing the active adsorption sites, thus ameliorating the limit of pore diffusion. For the adsorptive membrane, the characteristic diffusion length is on the scale of nanometers rather than micrometers. Thus, the external film diffusion rate is less of a mass transfer resistance compared to that of the larger porous particulates. This reduces the time required for solutes to transfer to active sites,[40,41] and it increases the overall capture efficiency and throughput capabilities of the process. Furthermore, though not a focus of this study, advances are being made in polymer engineering[42] to increase the adsorption capacity of adsorptive membranes to make them competitive with porous adsorptive particulates.

The objective of this study was to assess the mass transfer performance of a porous adsorptive membrane for removing PFAS from drinking water under varying conditions. While extensive research has been conducted on the use of membranes for PFAS removal,[43] the focus has primarily been on nanofiltration and reverse osmosis membranes, which rely on rejection by size exclusion. Adsorptive membranes have received comparatively less attention,[44] with most research focused on material advancements geared toward increasing adsorption capacity and selectivity (e.g. refs 45−47). While achieving substantial capacities for multiple PFAS is crucial, it is important to note that such considerations might be somewhat forward thinking. Equally critical is the confirmation

https://doi.org/10.1021/acsestengg.3c00515
ACS EST Engg. 2024, 4, 995−1006

that porous adsorptive membranes fulfill the promised reduction in mass transfer limitations.

In this study, we selected a commercially available porous polyamide membrane as a proof-of-concept adsorbent for PFAS removal. We chose polyamide as a model adsorptive membrane because it consists of a hydrophobic backbone interspersed with amide groups that may hydrolyze to form ionizable amines and carboxylic acids. This hydrophobic/electrostatic duality has demonstrated promising results for removing PFAS by ion exchange resins[20,26,31,38,48−51] and adsorbents functionalized with amines.[52] Our investigation focused on systematically examining the impact of various parameters on the dynamic adsorption performance of the adsorptive membrane. These parameters encompassed the chemistry of different PFAS, the contact time, the pH, the ionic strength (IS), and the presence of dissolved organic carbon (DOC). Outcomes were used to gain a comprehensive understanding of the mass transfer in a porous adsorptive membrane and how PFAS chemistry and water quality conditions affected the adsorption and mass transfer performance. This knowledge is crucial for validating the potential of the porous membrane structure for adsorption, improving the molecular engineering of adsorptive membranes, and optimizing operational strategies for adsorptive membrane systems targeting the removal of PFAS from drinking water.

2. EXPERIMENTAL APPROACH AND MODELING

2.1. Chemicals and Materials. All chemicals used in this study were purchased and used as received (further details are provided in the Supporting Information). The polyamide membrane was a porous, microfiltration membrane with a nominal pore size of 0.45 μm (Cytiva, 7404-002, 25 mm diameter). All stock solutions and samples were prepared with ultrapure water (18.2 MΩ·cm). The stock solutions for PFOA, PFOS, PFBS, and GenX were prepared in 1 L of high density polyethylene bottles that were free of fluorine.

2.2. Membrane Material Characterization. The polyamide membrane was characterized by several techniques, including Brunauer−Emmett−Teller (BET) surface area analysis, zeta potential analysis, scanning electron microscopy (SEM), porosity measurements, and permeability measurement.

BET was used to obtain the specific surface area (a, $m^2\ g^{-1}$) for use in adsorption performance characteristics. It was obtained through a physisorption experiment using N_2 in a volumetric adsorption system (Micromeritics ASAP 2020) operated at 77 K. Briefly, seven pristine polyamide membranes were cut into small pieces and loaded into a system vial. Subsequently, the system was degassed at 125 °C for 15 h. Then, the sample was pumped with N_2 at relative pressures ranging from 0.07 to 0.25 in liquid nitrogen. The resulting adsorption isotherm for N_2 was fitted with the BET model to obtain the specific surface area of the membrane.

The zeta potential was analyzed as a surrogate measure of the surface charge of the polyamide membrane over various pH ranges. An electrokinetic analyzer (Anton Paar SurPASS 3) was used to determine the zeta-potential of polyamide membrane samples with the streaming potential method. Before each trial, the polyamide membrane sample was soaked in ultrapure water for 12 h. At the beginning of each trial, two rectangles (each 2 cm × 1 cm) were cut from the membrane sample. The rectangles were then fixed into the adjustable gap cell of the SurPASS 3, and the distance between both rectangles in the measuring cell was set to 100 ± 10 μm. An electrolyte solution of 1 mM KCl was used for the zeta-potential measurements, and the pH was adjusted using 0.05 M HCl and 0.05 M NaOH solutions to achieve pH values between 3 and 10. For each trial, the membrane sample would begin with the electrolyte solution at pH 3, and the pH was incrementally increased by one unit until pH 10 was achieved. Then, the pH was incrementally decreased by one unit until pH 3 was achieved. At every new pH value, the membrane sample was first rinsed with the electrolyte solution, and then three zeta-potential measurements were taken (48 total zeta-potential measurements for each trial). All zeta-potential measurements taken at a given pH, from all trials, were averaged together, and then plotted along with the 95% confidence interval based on the standard error of the measurements at the given pH from all trials conducted. A dye test was further corroborated the zeta potential analysis (see the Supporting Information for further details).

Cross-sectional SEM micrographs were analyzed to obtain the thickness and porosity of the membrane. Surface SEM micrographs were used to corroborate the porosity of the membrane by determining the pore space presented on the image. Selected membrane samples were imaged by using a field-emission scanning electron microscope (FEI-Magellan 400). The membrane samples for cross-sectional analysis were prepared by immersing them in liquid nitrogen until the liquid nitrogen stopped bubbling vigorously (~30 s), followed by freeze fracturing. All samples were sputter-coated with 3 nm of Pd/Au using a Leica EM ACE600 High Vacuum Sputter Coater to prevent sample charging during imaging. 5 keV and 13 pA were used to generate all the SEM micrographs.

Because the adsorptive membranes are porous, porosity (ε) measurements were key to calculating the pore volume treated (PVT), which describes the volume of solution treated per pore volume in the dynamic adsorption experiments. Two methods were used to determine porosity—(1) water mass differentiation and (2) image analysis of SEM micrographs.[53] The porosity of membrane was measured using water mass differentiation, as described previously.[54]

For the mass differentiation approach, the membrane sample was weighed dry, submerged in ultrapure water for 10 min, and then reweighed. Excess liquid not entrained in the pores was removed by dabbing the surface with a Kimwipe (Kimberly-Clark Professional, 34120) until the liquid absorbed on the membrane was no longer dripping in a vertical position. This was performed in triplicate. The difference between the dry and weight masses of the membrane was calculated to determine the mass of water uptake. The volume of water uptake was calculated by dividing the mass of water by the density of water (0.997 mg mm^{-3}). The volume of the water uptake was assumed to be equal to the pore volume. The porosity was then calculated by dividing the pore volume by the total volume of the membrane. ImageJ was used to estimate the porosity from the SEM micrographs. This method was used to corroborate the mass differentiation result. This process is described in detail in the Supporting Information.

The permeability of the membrane was analyzed to determine the applied pressure necessary for the experiments. It was measured using a 10 mL stirred cell (EMD Millipore Amicon 8003) connected to a custom-made 800 mL reservoir that allowed for extended permeability testing. The stirred cell and reservoir were filled with ultrapure water, and a 5.64 bar trans-membrane pressure was applied to the reservoir. The

https://doi.org/10.1021/acsestengg.3c00515
ACS EST Engg. 2024, 4, 995−1006

permeate solution was collected in a container that was rested on a balance, and the mass of the collected solution was recorded every 3 s for 90 s to regress the water flux. Hydraulic permeabilities were calculated by dividing water flux by the transmembrane pressure and membrane area.

2.3. Batch Adsorption Experiments and Modeling. Batch adsorption isotherm experiments were conducted to obtain the adsorption capacity of the membrane at equilibrium for various initial concentrations of PFAS. Experiments were conducted in 50 mL polypropylene vials (VWR, 10026-078). Ten different initial concentrations of each PFAS ranging from 0.12 to 24.15 μM for PFOS (88−17,505 μg L^{-1}), PFOA (59−12,468 μg L^{-1}), PFBS (73−7380 μg L^{-1}), and GenX (41−5426 μg L^{-1}) were prepared. A single membrane was placed in each vial and then filled with 50 mL of the selected PFAS and concentration. Samples were mixed for 24 h at 100 rpm on a rotating mixer. The solution was then separated from the membrane and stored at 4 °C for analysis.

The batch adsorption isotherm data of all PFAS were fit with the Langmuir model,[55] which is described as $q_e = \frac{Q_m K_L C_e}{1 + K_L C_e}$. Here, q_e (μmol g^{-1}) is the solid-phase concentration of the adsorbate, C_e is the adsorbate concentration in solution at equilibrium (μmol L^{-1}), Q_m is the maximum adsorption capacity (μmol g^{-1}), and K_L is the adsorption equilibrium constant (L μmol^{-1}). Data were also fitted with the Freundlich model as a comparison, which is described in detail in the Supporting Information.

2.4. Dynamic Adsorption Experiments and Modeling. Flow-through adsorption experiments were conducted to determine the dynamic adsorption performance of the membrane. Results were used to assess the adsorption kinetics, mass transfer, and breakthrough performance of the membrane. To conduct the dynamic adsorption experiments, a flow-through contactor that consisted of a syringe pump (NE-300, SouthPointe Surgical Supply), a 60 mL syringe (polypropylene, Air-Tite Products Co., INC., MLB60), and a syringe filter holder (PALL Corporation, 4320, 25 mm diameter) was used. The syringe pumps were oriented vertically with liquid flow moving from top to bottom to ensure even contact with and flow through the membrane. Samples were collected at timed intervals in 50 mL vials (polypropylene, VWR, 10026-078).

Variables investigated in these experiments included PFAS type, contact time (or flow rate), pH, IS, and presence of DOC. The baseline conditions for each experiment were PFOS (3.62 μM), a flow rate of 5 mL min^{-1}, a pH of 6.8, and an IS of ∼3.6 μM (i.e., no added IS). Each variable was tested individually while keeping the other baseline variables constant.

Four PFAS were tested at an initial concentration of ∼3.62 μM, including PFOA (1800 μg L^{-1}), PFOS (2446 μg L^{-1}), PFBS (1589 μg L^{-1}), and GenX (1173 μg L^{-1}). A higher initial concentration was chosen to reduce the volume required to obtain a full breakthrough curve (BTC) profile.

To achieve varying contact times, the flow rate was adjusted from 2 to 20 mL min^{-1}. The calculated contact times (t_c), "empty-bed" contact times (EBCTs), superficial velocities (v_s), and pore velocities (v_i) are listed in Table 1. The contact time is analogous to the theoretical pore residence time in the membrane. The superficial velocities tested (∼0.2 to 2 m h^{-1}) were faster than those used for porous adsorptive particulates in fixed beds, which typically range from approximately 5 to 10 m h^{-1} (v_i = 11−22 m h^{-1}).[56] Similarly, the EBCTs tested herein were orders lower than EBCTs of fixed bed contactors containing GAC or IX resin, which range from 5 to 40 min.[50,57,58]

Table 1. Flow Rates Tested and the Corresponding Contact Time (t), EBCT, Superficial Velocity (v_s), Pore Velocity (v_i), and Applied Pressure (ΔP) for a Membrane Area of 4.9 cm^2, Thickness of 166 μm, and Porosity of 0.37

Q (cm^3 min^{-1})	t_c (s)	EBCT (s)	v_s (m h^{-1})	v_i (m h^{-1})	ΔP (psi)
2	0.90	2.4	0.24	0.66	0.34
5	0.36	0.98	0.61	1.7	0.84
10	0.18	0.49	1.2	3.3	1.69
20	0.09	0.24	2.4	6.6	3.38

Finally, the effects of pH, IS, and DOC were evaluated to probe the changes in membrane and water chemistry on the dynamic adsorption performance. The effect of pH was tested by adding either hydrochloric acid or sodium carbonate/bicarbonate to adjust the pH to approximately 3 and 11, respectively. The effect of the IS was explored by comparing the performance of the baseline IS to a solution adjusted to 0.5 M with sodium chloride. The effect of DOC was tested using a model humic acid sodium salt at 24.7 mg C L^{-1} (Sigma-Aldrich H16752). The DOC/PFOS was mixed for 2 min on a shaker plate before the dynamic adsorption experiment. The specific ultraviolet absorbance at 254 nm (SUVA254) was determined by using a UV−vis spectrophotometer (Hach DR5000).

The dynamic adsorption experiments produced data sets used to make BTCs. The BTCs were plotted as the normalized concentrations (C/C_0) as a function of the number of PVT, where C is the effluent concentration at time t and C_0 is the influent concentration. PVT is described in eqs 1 and 2.

$$V_p = V_m \varepsilon \tag{1}$$

$$\text{PVT} = \frac{V_t}{V_p} \tag{2}$$

where V_p is the pore volume (mm^3), V_m is the membrane volume (mm^3), ε is the membrane porosity, and V_t is the volume of solution treated (mm^3). The contact time (t_c) was calculated in terms of V_p and flow rate (Q) using eq 3. The t_c range of the dynamic adsorption experiments ranged from 0.09 to 0.9 s.

$$t_c = \frac{V_p}{Q} \tag{3}$$

To obtain comparable performance parameters and to allow integration of the BTC to obtain the mass of PFAS retained on the membrane, the BTCs were fitted with a sigmoidal model provided in eq 4.

$$\frac{C}{C_0} = A_1 + \frac{A_1 + A_2}{1 + 10^{(\log x_0 - x)m}} \tag{4}$$

where A_1 is the lower C/C_0 plateau, A_2 is the upper C/C_0 plateau, x is the PVT, and x_0 is the PVT where A_1/A_2 = 0.5; when A_1 = 0 and A_2 = 1, x_0 is at a C/C_0 = 0.5. For fitting purposes, A_1 was constrained to 0.

2.5. Analytics. PFAS concentrations were quantified using ultraperformance liquid chromatography coupled with a triple quadrupole mass spectrometer (LC-MS/MS; Agilent 1290

https://doi.org/10.1021/acsestengg.3c00515
ACS EST Engg. 2024, 4, 995−1006

Infinity II and G6475AA) using an electrospray ion source (G1948B) operated in negative ion mode. Polytetrafluoroethylene-free fittings and lines were used throughout the system. ACS grade eluents were used, filtered through a 0.45 μm polyether sulfone membrane. 300 μL polypropylene vials and caps (Microsolv, 97052-662) were used for sample handling. PFAS were separated on a ZORBAX RRHD Eclipse Plus column (Agilent 959758-902; C18, 95 Å, 2.1 × 100 mm, 1.8 μm, 1200 bar). The column was kept at 40 °C with the gradient elution flow rate of 0.4 mL min^{-1} for 17 min. The sample injection volume was 10 μL. The gradient elution was started with a solvent mixture of 90% ultrapure water and 10% methanol for 1 min. After 1 min, the methanol concentration was increased to 40% and reached 90% linearly for 25 min. After 25 min, the methanol concentration was decreased to 10% and the concentration was decreased for 1 min. A delay column (Waters Atlantis T3, 186003734; 100 Å, 5 μm, 2.1 mm × 50 mm) that sits between the solvent mixer and the injector was used to separate PFAS impurities from the solvents. Inlet filters (12−14 μm, SST, Agilent, 01018-60025) were used for each of the solvents to remove any particulates and reduce a bubble formation.

3. RESULTS AND DISCUSSION

3.1. Material Characterization of the Membrane. The specific surface area of the membrane was 10.8 m^2 g^{-1}, as determined by the BET analysis. This is approximately 2 orders of magnitude lower than commercially available GAC. Figure 2 shows the zeta potential analysis of the membrane at various pH. The isoelectric point (IEP) was approximately 4.39. Presumably, chargeable carboxylate and amine groups exist within the membrane from either mild hydrolysis of the amide groups or the presence of end groups.[59−62] At pH less than the IEP, the carboxylate and amine groups would be predominately protonated to give the membrane a net positive charge. At a pH greater than the IEP, a net negative charge is present from the deprotonated carboxylic groups. The zeta potential outcome was corroborated by a dye test. At a pH of 3, when the membrane was predominantly positively charged, no adsorption of methylene blue (MB) (cationic) was observed, while approximately 25% of acid green 25 (AG) (anionic) was absorbed. At a pH of 10, when the membrane was predominantly negatively charged, the opposite was observed: 35% of MB adsorbed, whereas no AG adsorption occurred. Thus, at acidic pH, the adsorption of anionic PFAS should be more favorable if the attachment is controlled by electrostatic interactions. Under alkaline conditions, very little PFAS should be absorbed unless hydrophobic interactions are also playing a role in the attachment.

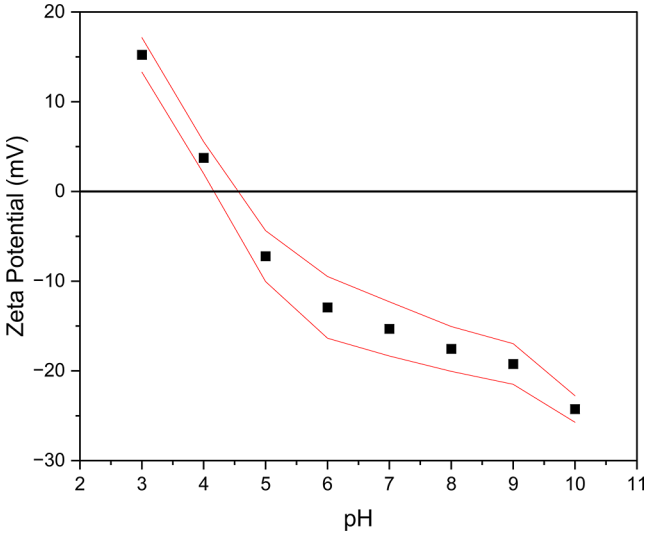

Figure 2. Zeta potential of the polyamide microfiltration membrane. An electrolyte solution of 1 mM KCl was used, and the pH 3−10 was adjusted automatically by the apparatus using 0.05 M HCl and 0.05 M NaOH solutions. 95% confidence intervals.

The thickness of the membrane was approximately 166 μm, as determined from the cross-sectional image of the SEM micrographs (Figure S2). The porosity of the membrane was measured as 0.37 using the water mass differentiation method, which was confirmed by SEM analysis (0.36). The pore area of the membrane was calculated by multiplying the porosity and membrane area, and the pore volume was calculated by multiplying the porosity and membrane volume. For a membrane sample with a 25 mm diameter, these were 182 mm^2 and 30.2 mm^3, respectively. The pore volume was used to calculate the PVT, which describes the volume of solution treated per pore volume. PVT was used to evaluate the performance of the membrane for the dynamic adsorption experiments. The permeability was measured as 1.05 × 10^4 L m^{-2} hr^{-1} bar^{-1}.

3.2. Batch Adsorption Isotherms. Figure 3 shows the batch adsorption isotherms for PFOS, PFOA, PFBS, and GenX on the polyamide membrane. The adsorption data of all PFAS were fitted with the Langmuir and Freundlich models.[55] Table 2 (mass) and Table S1 (molar) list the fitted Langmuir and Freundlich model parameters. The sum of squared errors (SSE) of the models was similar, but the Langmuir model was more representative of the plateauing of q_e at high C_e values

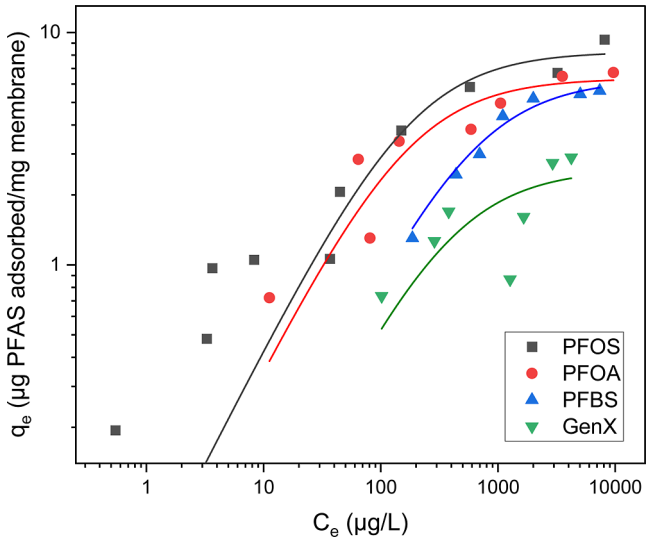

Figure 3. Batch adsorption isotherms for PFOS, PFOA, PFBS, and GenX onto the polyamide microfiltration membrane. The pH values of these solutions were 6.8, 5.9, 5.3, and 5.5, respectively. The membrane sample (mass = 20.8 mg) and 50 mL of the solution with concentrations ranging from 0.12 to 24.15 μM PFOS (88−17,505 μg L^{-1}), PFOA (59−12,468 μg L^{-1}), PFBS (73−7380 μg L^{-1}), and GenX (41−5426 μg L^{-1}) were mixed for 24 h at 100 rpm on a rotating mixer. The lines are the fitted with the Langmuir model.

https://doi.org/10.1021/acsestengg.3c00515
ACS EST Engg. 2024, 4, 995−1006

Table 2. Nonlinear Regressed Langmuir and Freundlich Parameters for PFOS, PFOA, PFBS, and GenX[a]

PFAS	Langmuir			Freundlich		
	K_L (L mg^{-1})	Q_m (μg mg^{-1})	SSE	K_F (μg mg^{-1}) (L/μg)$^{1/n}$	$1/n$	SSE
PFOS	5.4×10^{-3}	8.26	4.5	0.73	0.28	4.3
PFOA	5.8×10^{-3}	6.34	4.1	0.88	0.23	3.8
PFBS	1.6×10^{-3}	6.28	1.1	0.49	0.28	3.3
GenX	2.6×10^{-3}	2.58	2.4	0.14	0.36	1.6

[a]Molar based concentrations are listed in Table S2.

and was thus selected as the representative isotherm model. Using the Langmuir model suggests that the adsorption of PFAS to the polyamide membrane occurs on single sites of equal energy until a monolayer forms and that the PFAS are noninteracting on the surface. It is also possible that the data fit a pseudo-Langmuir model, meaning the Langmuir model is simply a good empirical fit without providing insights into the adsorption mechanisms.

PFOS had the greatest affinity (K_L) for the membrane (2.70×10^{-3} L nmol^{-1}), though it was similar to PFOA (2.39×10^{-3} L nmol^{-1}). The affinities of GenX (8.42×10^{-4} L nmol^{-1}) and PFBS (4.77×10^{-4} L nmol^{-1}) were approximately 5× lower. The additional CF_2 groups in the longer chain PFAS (PFOS and PFOA) shift more electron density to the tail, which results in a more hydrophobic tail[37] and a more easily ionizable and slightly stronger acid headgroup. Thus, the greater affinity associated with the long-chain PFAS could be due to either increased hydrophobic interactions with the polyamide backbone or increased attractive electrostatic interactions with the charged groups on the polyamide.[39,50,63] Though the affinities of PFOS/PFOA and PFBS were different, the molar-based maximum adsorption capacities (Q_m) (Figure S3) were similar, ranging from ∼15 to 21 nmol mg^{-1}. This suggests that under these experimental conditions PFOS, PFOA, and PFBS attached to and saturated similar adsorption sites. The affinity of GenX was 1.8× greater than PFBS, but the capacity of PFBS was 2.7× greater than GenX. GenX is a six carbon PFAS with the center CF_2 replaced by an ether. This would reduce both the hydrophobicity in the tail and the acidity in the head, resulting in reduced interactions between GenX and the polyamide membrane.

3.3. Dynamic Adsorption: Effect of PFAS Chemistry.

The BTCs for the dynamic adsorption of PFOS, PFOA, PFBS, and GenX onto the membrane are shown in Figure 4 and modeling results are provided in Table S2. The PVT values at C/C_0 = 0.05, 0.1, 0.5, 0.9, and 0.95 are also listed in the table. The PVT at C/C_0 = 0.5 ($PVT_{0.5}$) was used to compare the experimental outcomes. The $PVT_{0.5}$ values for PFOS, PFOA, PFBS, and GenX were 2056, 1489, 1540, and 760, respectively. The breakthrough performance, as indicated by $PVT_{0.5}$, was greater for PFOS compared to the other PFAS tested. This outcome was consistent with the trends observed in the isotherm results (Figure 3). For GenX, a structure similar to a perfluorinated carboxylic acid with an ether substituted CF_2, its $PVT_{0.5}$ was approximately 50% less than that of PFOA, which emphasizes how minor changes in the tail chemistry can impact the adsorption performance considerably. Specifically, the exchange of a CF_2 for an O will reduce both the hydrophobicity of the tail and electrostatic potential of the headgroup, thus reducing the affinity to the membrane. Similarly, the $PVT_{0.5}$ for PFOA (7 carbon tail) and PFBS (4 carbon tail) were similar, further highlighting the affinity of the sulfonic headgroup for the membrane sites. The sulfonic group

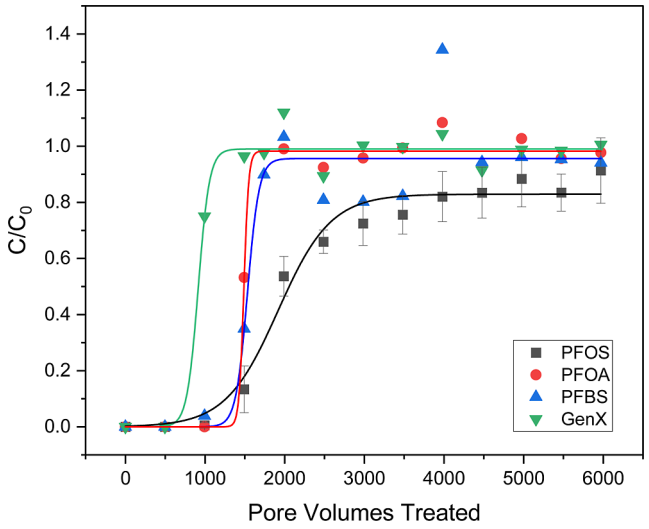

Figure 4. BTCs for PFOS, PFOA, PFBS, and GenX adsorption to the polyamide microfiltration membrane. 60 mL of PFOS (2446 μg L^{-1}), PFOA (1800 μg L^{-1}), PFBS (1589 μg L^{-1}), and GenX (1173 μg L^{-1}) were tested at the flow rate of 5 mL min^{-1}. Data were fitted with an empirical sigmoidal curve (eq 4). t_c = 0.36 s. The error bars of PFOS represent 1 standard deviation in each direction for triplicate runs.

is a relatively harder Lewis base than the carboxylic group, which would lead to increased attractive electrostatic interactions.[37] The PVT can also be expressed as a specific throughput for comparison to more conventional adsorbents; however, a key distinction is that this mass-based approach can be misleading due to variations in the adsorbent densities, surface area-to-volume ratios, and initial concentrations. Nevertheless, the specific throughput values for PFOS, PFOA, PFBS, and GenX at a C/C_0 = 0.5 were 3.0, 2.2, 2.2, and 1.3 (L_{water} $g_{membrane}^{-1}$), respectively.

The dynamic adsorption capacity (q_d; μg_{PFAS} per $mg_{membrane}$) was calculated by integrating the fitted curves of the BTCs. All values, including molar based units, are summarized in Table S2. The q_d values for PFOS, PFOA, PFBS, and GenX were 12.6 μg of PFOS mg^{-1}, 4.1 μg of PFOA mg^{-1}, 4.0 μg of PFBS mg^{-1}, and 1.6 μg of GenX mg^{-1}, respectively. Comparatively, the equilibrium capacities (q_e) obtained from the isotherm model at the influent C used in the dynamic adsorption tests were 7.8, 5.8, 4.5, and 1.9 μg of PFAS mg^{-1} for PFOS, PFOA, PFBS, and GenX, respectively.

The q_e represents the maximum mass that can be adsorbed at the influent concentration. In other words, it is not impacted by mass transfer resistances. However, in the dynamic adsorption tests, the interplay between the adsorption rate and mass transfer rates will impact the mass that can be adsorbed through the membrane or bed length. Except for PFOS, the q_d and q_e were similar for all PFAS, indicating that equilibrium capacities were capable at a rapid contact time

https://doi.org/10.1021/acsestengg.3c00515
ACS EST Engg. 2024, 4, 995−1006

(0.36 s) and that mass transfer resistances were minimal. Note that q_d and q_e are both calculated using the model parameters. In the model for q_d, A_2 indicates the upper plateau of the curve that is being integrated to obtain the mass adsorbed. If $A_2 < 1$, then the mass adsorbed will be overestimated, and if $A_2 > 1$, then the mass adsorbed will be underestimated. A_2 for PFOS was 0.89, so the overestimation of the q_d was due to modeling discrepancies. PFOS was the only PFAS that exhibited a more diffuse and nonideal BTC, in which mass transfer resistances are present. The length of the mass transfer zone (L_{MTZ}) for PFOS (90 μm) was approximately 6× longer than for PFOA (15 μm), which had the most ideal BTC (see the Supporting Information for calculation). All were less than the thickness of the membrane (166 μm).

The initial concentrations used in this study were higher than expected to be found in drinking water sources (i.e., less than 1 μg L^{-1}). The initial concentration will impact both mass transfer and adsorption capacity, where lower concentrations will result in a slow diffusive mass transfer and lower adsorption capacity. Figure S5 shows the BTC for PFOA at a C_0 of 98 μg L^{-1}. The $PVT_{0.5}$ of the low C_0 run (6033) was much higher than the high C_0 run (1489) due to the decrease in influent mass; however, because of the reduced driving force for mass transfer and adsorption, the q_d was about half the q_e (2.3 μg mg^{-1}).

3.4. Dynamic Adsorption: Effect of Contact Time. Figure 5 shows the BTCs for PFOS adsorption to the membrane at various contact times. Increasing the contact time from 0.09 to 0.9 s increased the $PVT_{0.5}$ from 1704 to 2120 and the q_d from 10.4 to 12.5 μmol g^{-1}, indicating very little performance loss when decreasing the contact time an order of magnitude. A contact time of 0.09 s in the membrane tested herein corresponds to a v_i of 0.66 m h^{-1} (Table 1). By comparison, the shortest v_i typically observed in GAC packed beds is ~11 m h^{-1}.[56] Operationally, the ability to implement shorter contact times allows for smaller footprints and reduced capital costs. Overall, the similar performance across an order of magnitude of v_i supports the notion that mass transfer is a minor limitation in the adsorptive membrane.

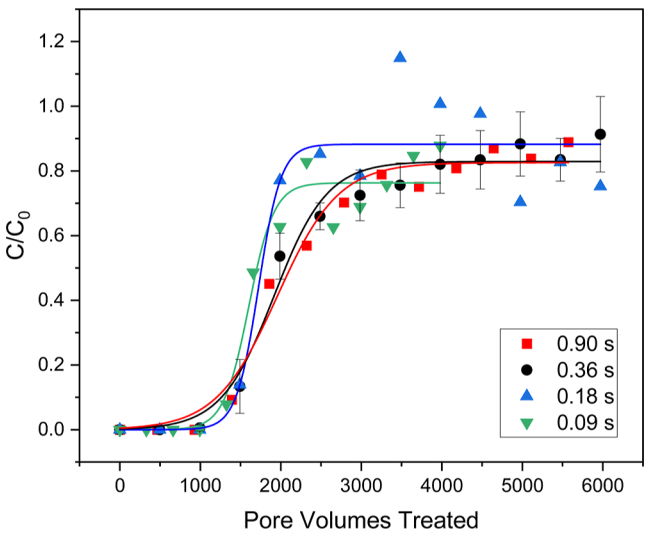

Figure 5. BTCs for PFOS adsorption to the polyamide microfiltration membrane at varying contact times. The pH was 6.8, and the IS was 3.6 × 10^{-6} M. The error bars of 0.36 s represent 1 standard deviation in each direction for triplicate runs.

3.5. Dynamic Adsorption: Effect of pH and Ionic Strength. pH and IS are critical water quality parameters that can impact the adsorption capacity and kinetics. They are also useful variables to probe to provide insights into the underlying adsorption mechanisms. Figure 6 shows the BTCs for PFOS adsorption to the membrane at different pH and IS. The native pH and IS of the PFOS solution under the baseline conditions were approximately 6.8 and IS of 3.6 × 10^{-6} M, respectively ($PVT_{0.5}$ = 2056, q_d = 12.6 μg mg^{-1}). Two additional pHs of 3 and 10.9 were tested under native IS and at an IS of 5 × 10^{-1} M. The native IS were relatively low but higher than the baseline conditions due to the required ion addition to adjust the pH (IS at pH 3 = 1 × 10^{-3} M and IS at pH 10.9 = 1 × 10^{-2} M).

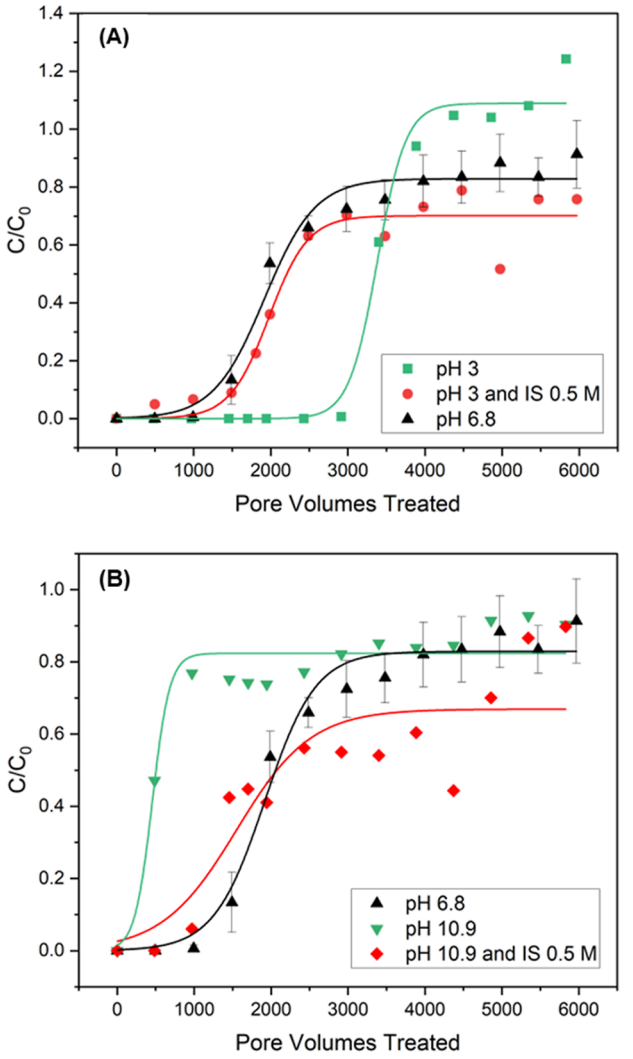

Figure 6. BTCs for PFOS adsorption to the polyamide microfiltration membrane at (A) pH 3 and (B) pH 10.9 with either native IS or an IS of 5 × 10^{-1} M. The error bars of pH 6.8 represent 1 standard deviation in each direction for triplicate runs.

At a pH of 3 (Figure 6A) and an IS of 1 × 10^{-3} M, an improvement in the breakthrough performance was observed compared to the baseline condition, with the $PVT_{0.5}$ and q_d increasing to 3352 and 15.4 μg mg^{-1}, respectively. At pH 3

https://doi.org/10.1021/acsestengg.3c00515
ACS EST Engg. 2024, 4, 995−1006

with an IS of 5×10^{-1} M, the $PVT_{0.5}$ and q_d were reduced to 2208 and 14.7 $\mu g\ mg^{-1}$, respectively, which was similar to the baseline conditions. At a pH of 10.9 and IS of 1×10^{-2} M, compared to the baseline experiment the $PVT_{0.5}$ and q_d decreased to 505 and 6.0 $\mu g\ mg^{-1}$, respectively (Figure 6B). Increasing the IS to 5×10^{-1} M for a pH of 10.9 improved the $PVT_{0.5}$ and q_d to 2076 and 13.1 $\mu g\ mg^{-1}$, respectively.

At acidic and alkaline conditions, increasing the IS reverted the adsorption performance to circumneutral baseline conditions. At pH of 3 and 10.9, the polyamide membrane would be positively and negatively charged, respectively (IEP = 4.39, Figure 2). If only the effect of pH is considered, the dominant adsorption mechanism between PFOS and the polyamide membrane is presumably the electrostatic attraction between the sulfonic headgroup and positively charged amine sites. This was evident by the increase in adsorbed PFOS at pH 3 and the decrease at pH 10.9. However, IS also plays a role in adsorption. Increasing the IS will diminish electrostatic interactions, both attractive and repulsive. When the membrane surface is dominated by positive charges (i.e., pH < IEP; pH = 3), anions along with co-occurring cations will populate the electric double layer (EDL). Increasing the IS will compress the EDL and the electrostatic attraction between the positive charges on the membrane and the PFOS headgroup will be shielded, thus reducing the amount adsorbed. This was observed when the membrane was tested at pH 3 and high IS. When the membrane surface is dominated by negative charges (i.e., pH > IEP; pH = 10.9), the negatively charged headgroup of PFOS will be repelled from the surface of the membrane. At high IS, the shielding effect will reduce the repulsive forces between the headgroups of PFOS and the membrane, and presumably this would permit the tail of PFOS to get close enough to the membrane that it can attach via hydrophobic interactions. This would also reduce the PFOS−PFOS (i.e., adsorbate−adsorbate) repulsive forces on the membrane surface, allowing them to aggregate for greater adsorption capacity. This was observed when the membrane was tested at pH 10.9 and high IS. Similar behavior was observed by Tang et al. for PFOS adsorption to goethite.[63] Overall, these observations suggest that PFOS attaches to the polyamide membrane via both electrostatic and hydrophobic interactions, but the pH and IS conditions determine the mechanism that will dominate the interaction. At low pH, the adsorption mechanism is dominated by electrostatic attraction, and as pH increases, the dominant mechanism shifts to hydrophobic interactions.

These outcomes were confirmed by two additional dynamic adsorption experiments that were conducted. The first test was PFBS at an IS of 5×10^{-1} M and a pH of 5.8. PFBS is a short-chain PFAS, and thus the adsorption should be dominated by electrostatic attraction. Increasing the IS decreased the $PVT_{0.5}$ from 1540 to 908, further corroborating the dominance of electrostatic interactions (Figure 7). In the second test, the membrane was tested under baseline conditions for three consecutive runs with methanol rinses between runs (Figure S4). The hypothesis was that methanol would wash off the hydrophobically bound PFOS while the electrostatically bound PFOS would remain. After rinsing, breakthrough in the second and third runs occurred sooner compared to the first run, indicating that a significant portion of the PFOS remained on the membrane from the previous run. Additionally, a marked chromatographic effect was observed in the second and third runs due to the flushing of PFOS that was still bound to the membrane. Some PFOS was washed off, which suggests that both electrostatic and hydrophobic interactions play a role in the adsorption of PFOS to the membrane. In practice, the regeneration of the adsorptive membranes should be capable of removing both hydrophobically and electrostatically bound PFAS (e.g., 5% NH_4OH in methanol[64]).

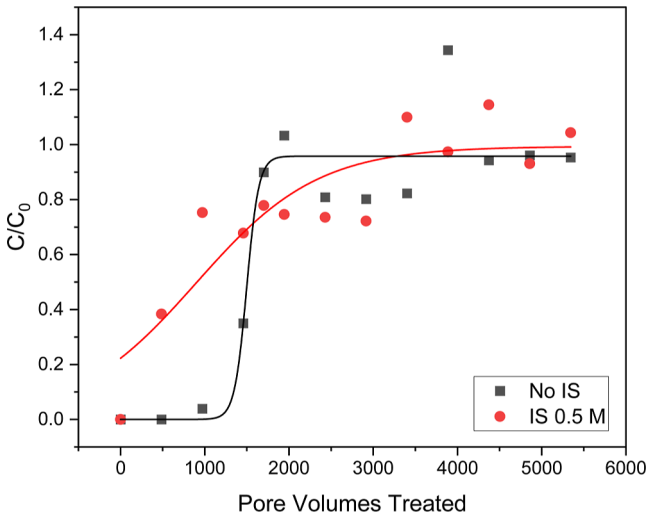

Figure 7. BTCs for PFBS adsorption to the polyamide microfiltration membrane at native pH and an IS of either native IS or IS of 5×10^{-1} M.

3.6. Dynamic Adsorption: Effect of DOC. Figure 8 shows the BTCs for the adsorption of PFOS to the membrane in the absence and presence of DOC (24.7 mg C L^{-1}; SUVA254 = 0.96 L mg C^{-1} m^{-1}) at various pH and IS. In the presence of DOC, the breakthrough performance was reduced considerably, with a decrease in the $PVT_{0.5}$ and q_d to 595 and 2.5 $\mu g\ mg^{-1}$, respectively. Due to the presence of negatively charged and hydrophobic groups, DOC can compete with PFAS for adsorption sites.[37] The competitiveness between DOC and PFOS for sites may depend on a molecular weight.[65] The majority of the DOC used in this study was 20−50 kDa,

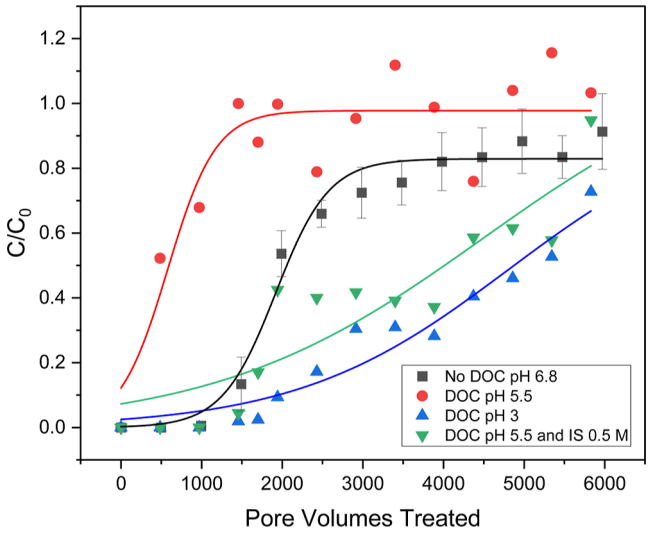

Figure 8. BTCs for PFOS adsorption to the polyamide microfiltration membrane in the presence of DOC at varying pH and IS. The error bars of pH 6.8 represent 1 standard deviation in each direction for triplicate runs.

https://doi.org/10.1021/acsestengg.3c00515
ACS EST Engg. 2024, 4, 995−1006

with sizes as small as 0.2 kDa, and PFOS is 0.5 kDa. Via the Vroman effect, the larger DOC will tend to displace and outcompete PFOS for adsorption sites. However, this displacement effect is typically only relevant for equilibrium processes that take the order of magnitude more time than the contact time used herein (0.36 s). A more likely explanation is the interaction between PFOS and DOC in solution via electrostatic and/or hydrophobic mechanisms as well as DOC populating the EDL and shielding PFOS from interacting with the membrane.[64] The DOC used in this study has aromatic structures and contains charged functional groups (e.g., amine, carboxylic), and the molar concentration is approximately 2 orders higher than PFOS. When it binds to the membrane, it can reduce the capacity for PFOS by either reducing the number of available adsorption sites or through repulsive forces from the anionic functional groups.[66,67] The additional negative charges provided by the DOC to the membrane would increase the apparent IEP,[37,65,68] thus reducing the net attractive forces available to bind PFOS. When the pH was decreased to 3, the adsorption performance improved, negating the effects of DOC, and increasing IS to 5×10^{-1} M had a minimal impact on the adsorption.

3.7. Implications for Material Design and Operation.

The diffusive mass transfer limitation of conventional particulate adsorbents in fixed beds is a major drawback because it leads to poor capture efficiencies and necessitates long contact times that ultimately increase operating costs. This study showed that adsorptive membranes have minor mass transfer limitations for removing PFAS from water. While adsorptive membranes that take advantage of this preferential mass transfer have been produced in several ways (e.g., molecular imprinting,[69,70] layer-by-layer deposition,[71−74] and grafting-to[75,76] or -from[77−79]), they tend to have relatively low total binding capacities compared to porous particulates.[69,70,80−82] Emerging techniques can address this technical gap,[42,83,84] making this adsorption platform an attractive option for removing PFAS from water. For example, Wan et al.[47] reported on a quaternized membrane capable of achieving a Q_m approximately 35 times greater than the membrane tested herein. To account for water chemistry, for anionic PFAS, the membrane design should incorporate permanently positively charged sites unaffected by pH, and the pore size and chemistry should be such that it does not preferentially adsorb DOC.

The commercial porous polyamide membranes used in this study were not specifically designed to have a high capacity for PFAS, but their site density for PFAS was surprisingly high. Calgon F400 GAC has a specific surface area of ∼1050 $m^2\ g^{-1}$, as reported by the manufacturer, and the Q_m for F400 has been reported as 236 mg g^{-1} for PFOS.[85] Using the values, we calculated a site density for PFOS of 22 ng cm^{-2} was calculated. In comparison, the site density of the membrane used herein, as calculated from a specific surface area of 10.8 $m^2\ g^{-1}$ and a Q_m of 8.26 mg g^{-1}, was 76 ng cm^{-2}. So, while porous particulates take advantage of high surface areas, they tend to have lower site densities.

From an operational standpoint, the adsorptive membrane platform is suited to tackle the diverse chemical range of PFAS that may be present in drinking water. They can be engineered to target anionic, cationic, and neutral PFAS with both short- and long-chain structures. Alao, their modular form permits stacking within the treatment process design, allowing for tailored removal strategies. For instance, pairing a positively charged membrane with a negatively charged one removes anionic and cationic PFAS, respectively. Similar to IX resins, these adsorptive membranes can be regenerated and reused, thus prolonging their service lifetime and reducing operational costs; however, questions remain about the feasibility of regeneration compared to single use and the costs associated with each approach. As with all adsorbents, DOC and competing constituents will decrease capacity, and this presents a challenge for the design and operation of adsorptive membranes, as its presence may necessitate costly pretreatments. Additionally, to compete with cost-effective solutions such as GAC and IX resin, advancements will be needed to reduce manufacturing costs of the membranes.

■ ASSOCIATED CONTENT

Supporting Information

The Supporting Information is available free of charge at https://pubs.acs.org/doi/10.1021/acsestengg.3c00515.

List of chemicals used in this study, additional BTCs, the dye test results and methods, the porosity analysis method, SEM images, alternative isotherm modeling, and a table summarizing the dynamic adsorption experiment results (PDF)

■ AUTHOR INFORMATION

Corresponding Author

Kyle Doudrick − *Department of Civil and Environmental Engineering and Earth Sciences, University of Notre Dame, Notre Dame, Indiana 46556, United States;* orcid.org/0000-0003-1912-9819; Phone: 574-631-0305; Email: kdoudrick@nd.edu

Authors

Jeein Kim − *Department of Civil and Environmental Engineering and Earth Sciences, University of Notre Dame, Notre Dame, Indiana 46556, United States;* orcid.org/0009-0000-1530-1314

Liliya Chernysheva − *Department of Civil and Environmental Engineering and Earth Sciences, University of Notre Dame, Notre Dame, Indiana 46556, United States*

Jialing Xu − *Department of Chemical and Biomolecular Engineering, University of Notre Dame, Notre Dame, Indiana 46556, United States*

Matthew McClure − *Department of Chemical Engineering, McMaster University, Hamilton, Ontario L8S 4L8, Canada*

David R. Latulippe − *Department of Chemical Engineering, McMaster University, Hamilton, Ontario L8S 4L8, Canada;* orcid.org/0000-0003-2873-0606

William A. Phillip − *Department of Chemical and Biomolecular Engineering, University of Notre Dame, Notre Dame, Indiana 46556, United States;* orcid.org/0000-0001-8871-585X

Complete contact information is available at: https://pubs.acs.org/10.1021/acsestengg.3c00515

Author Contributions

Jeein Kim investigation leader, data analysis, writing, editing. **Liliya Chernysheva** LC-MS/MS analysis. **Jialing Xu** membrane characterization. **Matthew McClure** zeta potential analysis. **David R. Latulippe** zeta potential analysis. **William A. Phillip** conceptualization, writing. **Kyle Doudrick** conceptualization, writing.

https://doi.org/10.1021/acsestengg.3c00515
ACS EST Engg. 2024, 4, 995−1006

Notes

The authors declare no competing financial interest.

■ ACKNOWLEDGMENTS

Support for this research was primarily provided by the National Science Foundation (NSF) grants CBET-1847466 (Doudrick) and CBET-1924715 (Phillip). The University of Notre Dame thanks ND Energy Materials Characterization Facility for use of the volumetric adsorption system, the Notre Dame Integrated Imaging Facility for use of the SEM, and the Mass Spectrometric and Proteomics Facility for use of the LC-MS/MS. McMaster University thanks the Centre of Excellence in Protective Equipment and Materials (CEPEM) for providing access to their electrokinetic analyzer.

■ REFERENCES

(1) USEPA. CompTox Chemicals Dashboard Master List of PFAS. 2019. https://comptox.epa.gov/dashboard/chemical-lists/PFASMASTER (accessed October 19, 2023).
(2) Hekster, F. M.; Laane, R.; de Voogt, P. Environmental and Toxicity Effects of Perfluoroalkylated Substances. *Rev. Environ. Contam. Toxicol.* **2003**, *179*, 99−121.
(3) Houde, M.; Martin, J. W.; Letcher, R. J.; Solomon, K. R.; Muir, D. C. G. Biological Monitoring of Polyfluoroalkyl Substances: A Review. *Environ. Sci. Technol.* **2006**, *40* (11), 3463−3473.
(4) Fromme, H.; Tittlemier, S. A.; Volkel, W.; Wilhelm, M.; Twardella, D. Perfluorinated Compounds - Exposure Assessment for the General Population in Western Countries. *Int. J. Hyg. Environ. Health* **2009**, *212* (3), 239−270.
(5) Jensen, A. A.; Leffers, H. Emerging Endocrine Disrupters: Perfluoroalkylated Substances. *Int. J. Androl.* **2008**, *31* (2), 161−169.
(6) Zhang, T.; Sun, H.; Qin, X.; Gan, Z.; Kannan, K. PFOS and PFOA in Paired Urine and Blood from General Adults and Pregnant Women: Assessment of Urinary Elimination. *Environ. Sci. Pollut. Res.* **2015**, *22* (7), 5572−5579.
(7) Lam, N. H.; Cho, C. R.; Kannan, K.; Cho, H. S. A Nationwide Survey of Perfluorinated Alkyl Substances in Waters, Sediment and Biota Collected from Aquatic Environment in Vietnam: Distributions and Bioconcentration Profiles. *J. Hazard. Mater.* **2017**, *323*, 116−127.
(8) Kannan, K.; Corsolini, S.; Falandysz, J.; Fillmann, G.; Kumar, K. S.; Loganathan, B. G.; Mohd, M. A.; Olivero, J.; Wouwe, N. V.; Yang, J. H.; Aldous, K. M. Perfluorooctanesulfonate and Related Fluorochemicals in Human Blood from Several Countries. *Environ. Sci. Technol.* **2004**, *38* (17), 4489−4495.
(9) Baduel, C.; Mueller, J. F.; Rotander, A.; Corfield, J.; Gomez-Ramos, M. J. Discovery of Novel Per- and Polyfluoroalkyl Substances (PFASs) at a Fire Fighting Training Ground and Preliminary Investigation of Their Fate and Mobility. *Chemosphere* **2017**, *185*, 1030−1038.
(10) Dauchy, X.; Boiteux, V.; Bach, C.; Rosin, C.; Munoz, J. F. Per- and Polyfluoroalkyl Substances in Firefighting Foam Concentrates and Water Samples Collected near Sites Impacted by the Use of These Foams. *Chemosphere* **2017**, *183*, 53−61.
(11) Houtz, E. F.; Higgins, C. P.; Field, J. A.; Sedlak, D. L. Persistence of Perfluoroalkyl Acid Precursors in AFFF-Impacted Groundwater and Soil. *Environ. Sci. Technol.* **2013**, *47* (15), 8187−8195.
(12) Place, B. J.; Field, J. A. Identification of Novel Fluorochemicals in Aqueous Film-Forming Foams Used by the US Military. *Environ. Sci. Technol.* **2012**, *46* (13), 7120−7127.
(13) Moody, C. A.; Field, J. A. Determination of Perfluorocarboxylates in Groundwater Impacted by Fire-Fighting Activity. *Environ. Sci. Technol.* **1999**, *33* (16), 2800−2806.
(14) Hu, X. C.; Andrews, D. Q.; Lindstrom, A. B.; Bruton, T. A.; Schaider, L. A.; Grandjean, P.; Lohmann, R.; Carignan, C. C.; Blum, A.; Balan, S. A.; Higgins, C. P.; Sunderland, E. M. Detection of Poly- and Perfluoroalkyl Substances (PFASs) in US Drinking Water Linked to Industrial Sites, Military Fire Training Areas, and Wastewater Treatment Plants. *Environ. Sci. Technol. Lett.* **2016**, *3* (10), 344−350.
(15) Barber, J. L.; Berger, U.; Chaemfa, C.; Huber, S.; Jahnke, A.; Temme, C.; Jones, K. C. Analysis of Per- and Polyfluorinated Alkyl Substances in Air Samples from Northwest Europe. *J. Environ. Monit.* **2007**, *9* (6), 530−541.
(16) McMahon, P. B.; Tokranov, A. K.; Bexfield, L. M.; Lindsey, B. D.; Johnson, T. D.; Lombard, M. A.; Watson, E. Perfluoroalkyl and Polyfluoroalkyl Substances in Groundwater Used as a Source of Drinking Water in the Eastern United States. *Environ. Sci. Technol.* **2022**, *56* (4), 2279−2288.
(17) Teymoorian, T.; Munoz, G.; Vo Duy, S.; Liu, J.; Sauvé, S. Tracking PFAS in Drinking Water: A Review of Analytical Methods and Worldwide Occurrence Trends in Tap Water and Bottled Water. *ACS ES&T Water* **2023**, *3* (2), 246−261.
(18) USEPA. Proposed PFAS National Primary Drinking Water Regulation. 2023. https://www.epa.gov/system/files/documents/2023-04/PFAS%20NPDWR%20Public%20Presentation_Full%20Technical%20Presentation_3.29.23_Final.pdf (accessed October 19, 2023).
(19) Crone, B. C.; Speth, T. F.; Wahman, D. G.; Smith, S. J.; Abulikemu, G.; Kleiner, E. J.; Pressman, J. G. Occurrence of Per- and Polyfluoroalkyl Substances (PFAS) in Source Water and Their Treatment in Drinking Water. *Crit. Rev. Environ. Sci. Technol.* **2019**, *49* (24), 2359−2396.
(20) Maimaiti, A.; Deng, S.; Meng, P.; Wang, W.; Wang, B.; Huang, J.; Wang, Y.; Yu, G. Competitive Adsorption of Perfluoroalkyl Substances on Anion Exchange Resins in Simulated AFFF-Impacted Groundwater. *Chem. Eng. J.* **2018**, *348*, 494−502.
(21) McCleaf, P.; Englund, S.; Östlund, A.; Lindegren, K.; Wiberg, K.; Ahrens, L. Removal Efficiency of Multiple Poly- and Perfluoroalkyl Substances (PFASs) in Drinking Water Using Granular Activated Carbon (GAC) and Anion Exchange (AE) Column Tests. *Water Res.* **2017**, *120*, 77−87.
(22) Cantoni, B.; Turolla, A.; Wellmitz, J.; Ruhl, A. S.; Antonelli, M. Perfluoroalkyl Substances (PFAS) Adsorption in Drinking Water by Granular Activated Carbon: Influence of Activated Carbon and PFAS Characteristics. *Sci. Total Environ.* **2021**, *795*, 148821.
(23) Pauletto, P. S.; Bandosz, T. J. Activated Carbon versus Metal-Organic Frameworks: A Review of Their PFAS Adsorption Performance. *J. Hazard. Mater.* **2022**, *425*, 127810.
(24) Zeng, C.; Atkinson, A.; Sharma, N.; Ashani, H.; Hjelmstad, A.; Venkatesh, K.; Westerhoff, P. Removing Per- and Polyfluoroalkyl Substances from Groundwaters Using Activated Carbon and Ion Exchange Resin Packed Columns. *AWWA Water Sci.* **2020**, *2* (1), No. e1172.
(25) Park, M.; Wu, S.; Lopez, I. J.; Chang, J. Y.; Karanfil, T.; Snyder, S. A. Adsorption of Perfluoroalkyl Substances (PFAS) in Groundwater by Granular Activated Carbons: Roles of Hydrophobicity of PFAS and Carbon Characteristics. *Water Res.* **2020**, *170*, 115364.
(26) Boyer, T. H.; Fang, Y.; Ellis, A.; Dietz, R.; Choi, Y. J.; Schaefer, C. E.; Higgins, C. P.; Strathmann, T. J. Anion Exchange Resin Removal of Per- and Polyfluoroalkyl Substances (PFAS) from Impacted Water: A Critical Review. *Water Res.* **2021**, *200*, 117244.
(27) Fang, Y.; Ellis, A.; Choi, Y. J.; Boyer, T. H.; Higgins, C. P.; Schaefer, C. E.; Strathmann, T. J. Removal of Per- And Polyfluoroalkyl Substances (PFASs) in Aqueous Film-Forming Foam (AFFF) Using Ion-Exchange and Nonionic Resins. *Environ. Sci. Technol.* **2021**, *55* (8), 5001−5011.
(28) Wang, Y.; Darling, S. B.; Chen, J. Selectivity of Per- And Polyfluoroalkyl Substance Sensors and Sorbents in Water. *ACS Appl. Mater. Interfaces* **2021**, *13* (51), 60789−60814.
(29) Zhang, D.; He, Q.; Wang, M.; Zhang, W.; Liang, Y. Sorption of Perfluoroalkylated Substances (PFASs) onto Granular Activated Carbon and Biochar. *Environ. Technol.* **2021**, *42* (12), 1798−1809.
(30) Zhang, Z.; Sarkar, D.; Datta, R.; Deng, Y. Adsorption of Perfluorooctanoic Acid (PFOA) and Perfluorooctanesulfonic Acid (PFOS) by Aluminum-Based Drinking Water Treatment Residuals. *J. Hazard. Mater. Lett.* **2021**, *2*, 100034.

https://doi.org/10.1021/acsestengg.3c00515
ACS EST Engg. 2024, 4, 995−1006

(31) Wang, Y.; Warner, M.; Li, K.; Hawkins, G. L.; Huang, Q. Assessing Explicit Models of Per- and Polyfluoroalkyl Substances Adsorption on Anion Exchange Resins by Rapid Small-Scale Column Tests. *Chemosphere* **2022**, *300*, 134547.
(32) Kempisty, D. M.; Arevalo, E.; Spinelli, A. M.; Edeback, V.; Dickenson, E. R. V.; Husted, C.; Higgins, C. P.; Summers, R. S.; Knappe, D. R. U. Granular Activated Carbon Adsorption of Perfluoroalkyl Acids from Ground and Surface Water. *AWWA Water Sci.* **2022**, *4* (1), No. e1269.
(33) Patterson, C.; Burkhardt, J.; Schupp, D.; Krishnan, E. R.; Dyment, S.; Merritt, S.; Zintek, L.; Kleinmaier, D. Effectiveness of Point-of-Use/Point-of-Entry Systems to Remove per- and Polyfluoroalkyl Substances from Drinking Water. *AWWA Water Sci.* **2019**, *1* (2), No. e1131.
(34) Najm, I.; Gallagher, B.; Vishwanath, N.; Blute, N.; Gorzalski, A.; Feffer, A.; Richardson, S. Per- and Polyfluoroalkyl Substances Removal with Granular Activated Carbon and a Specialty Adsorbent: A Case Study. *AWWA Water Sci.* **2021**, *3* (5), No. e1245.
(35) Grieco, S. A.; Chang, J.; Maio, E. L. Y.; Hwang, M. Comparing Conventional and Emerging Adsorbents for Per- and Polyfluoroalkyl Substances: Kinetic, Equilibrium, and Column Experiments. *AWWA Water Sci.* **2021**, *3* (6), No. e1256.
(36) Wu, C.; Klemes, M. J.; Trang, B.; Dichtel, W. R.; Helbling, D. E. Exploring the Factors That Influence the Adsorption of Anionic PFAS on Conventional and Emerging Adsorbents in Aquatic Matrices. *Water Res.* **2020**, *182*, 115950.
(37) Du, Z.; Deng, S.; Bei, Y.; Huang, Q.; Wang, B.; Huang, J.; Yu, G. Adsorption Behavior and Mechanism of Perfluorinated Compounds on Various Adsorbents—A Review. *J. Hazard. Mater.* **2014**, *274*, 443−454.
(38) Murray, C. C.; Marshall, R. E.; Liu, C. J.; Vatankhah, H.; Bellona, C. L. PFAS Treatment with Granular Activated Carbon and Ion Exchange Resin: Comparing Chain Length, Empty Bed Contact Time, and Cost. *J. Water Process Eng.* **2021**, *44*, 102342.
(39) Zhang, D. Q.; Zhang, W. L.; Liang, Y. N. Adsorption of Perfluoroalkyl and Polyfluoroalkyl Substances (PFASs) from Aqueous Solution - A Review. *Sci. Total Environ.* **2019**, *694*, 133606.
(40) Zhang, Y. Z.; Almodovar-Arbelo, N. E.; Weidman, J. L.; Corti, D. S.; Boudouris, B. W.; Phillip, W. A. Fit-for-Purpose Block Polymer Membranes Molecularly Engineered for Water Treatment. *NPJ Clean Water* **2018**, *1*, 2.
(41) Zhang, Y.; Sargent, J. L.; Boudouris, B. W.; Phillip, W. A. Nanoporous Membranes Generated from Self-Assembled Block Polymer Precursors: Quo Vadis? *J. Appl. Polym. Sci.* **2015**, *132* (21), 41683.
(42) Zhang, Y.; Vallin, J. R.; Sahoo, J. K.; Gao, F.; Boudouris, B. W.; Webber, M. J.; Phillip, W. A. High-Affinity Detection and Capture of Heavy Metal Contaminants Using Block Polymer Composite Membranes. *ACS Cent. Sci.* **2018**, *4* (12), 1697−1707.
(43) Lu, D.; Sha, S.; Luo, J.; Huang, Z.; Zhang Jackie, X. Treatment Train Approaches for the Remediation of Per- and Polyfluoroalkyl Substances (PFAS): A Critical Review. *J. Hazard. Mater.* **2020**, *386*, 121963.
(44) Jin, T.; Peydayesh, M.; Mezzenga, R. Membrane-Based Technologies for per- and Poly-Fluoroalkyl Substances (PFASs) Removal from Water: Removal Mechanisms, Applications, Challenges and Perspectives. *Environ. Int.* **2021**, *157*, 106876.
(45) Johnson, J. K.; Michael Salerno, K.; Schlesinger, D. R.; Le, N. Q.; Ko, J. S.; Xia, Z. Removing Forever Chemicals via Amphiphilic Functionalized Membranes. *NPJ Clean Water* **2022**, *5*, 55.
(46) Kang, S. B.; Wang, Z.; Zhang, W.; Kim, K. Y.; Won, S. W. Removal of Short- and Long-Chain PFAS from Aquatic Systems Using Electrostatic Attraction of Polyethylenimine-Polyvinyl Chloride Electrospun Nanofiber Adsorbent. *Sep. Purif. Technol.* **2023**, *326*, 124853.
(47) Wan, H.; Fang, F.; Shi, K.; Yi, Z.; Lei, L.; Li, S.; Mills, R.; Bhattacharyya, D.; Xu, Z. PH-Swing Membrane Adsorption of Perfluoroalkyl Substances: Anion-Exchange Brushes and Role of Water Chemistry. *Sep. Purif. Technol.* **2024**, *329*, 124800.
(48) Deng, S.; Yu, Q.; Huang, J.; Yu, G. Removal of Perfluorooctane Sulfonate from Wastewater by Anion Exchange Resins: Effects of Resin Properties and Solution Chemistry. *Water Res.* **2010**, *44* (18), 5188−5195.
(49) Yu, Q.; Zhang, R.; Deng, S.; Huang, J.; Yu, G. Sorption of Perfluorooctane Sulfonate and Perfluorooctanoate on Activated Carbons and Resin: Kinetic and Isotherm Study. *Water Res.* **2009**, *43* (4), 1150−1158.
(50) Woodard, S.; Berry, J.; Newman, B. Ion Exchange Resin for PFAS Removal and Pilot Test Comparison to GAC. *Rem. J.* **2017**, *27* (3), 19−27.
(51) Du, Z.; Deng, S.; Chen, Y.; Wang, B.; Huang, J.; Wang, Y.; Yu, G. Removal of Perfluorinated Carboxylates from Washing Wastewater of Perfluorooctanesulfonyl Fluoride Using Activated Carbons and Resins. *J. Hazard. Mater.* **2015**, *286*, 136−143.
(52) Karoyo, A. H.; Wilson, L. D. Tunable Macromolecular-Based Materials for the Adsorption of Perfluorooctanoic and Octanoic Acid Anions. *J. Colloid Interface Sci.* **2013**, *402*, 196−203.
(53) AlMarzooqi, F. A.; Bilad, M. R.; Mansoor, B.; Arafat, H. A. A Comparative Study of Image Analysis and Porometry Techniques for Characterization of Porous Membranes. *J. Mater. Sci.* **2016**, *51* (4), 2017−2032.
(54) Gholap, S. G.; Musale, D. A.; Kulkarni, S. S.; Karode, S. K.; Kharul, U. K. Protein and Buffer Transport through Anionically Grafted Nylon Membranes. *J. Membr. Sci.* **2001**, *183*, 89−99.
(55) Langmuir, I. The Constitution and Fundamental Properties of Solids and Liquids. Part I. Solids. *J. Am. Chem. Soc.* **1916**, *38* (11), 2221−2295.
(56) Crittenden, J. C.; Rhodes Trussell, R.; Hand, D. W.; Howe, K. J.; Tchobanoglous, G. *MWH's Water Treatment: Principles and Design*, 3rd ed.; John Wiley & Sons, Inc., 2012.
(57) Riegel, M.; Haist-Gulde, B.; Sacher, F. Sorptive Removal of Short-Chain Perfluoroalkyl Substances (PFAS) during Drinking Water Treatment Using Activated Carbon and Anion Exchanger. *Environ. Sci. Eur.* **2023**, *35* (1), 12.
(58) Belkouteb, N.; Franke, V.; McCleaf, P.; Köhler, S.; Ahrens, L. Removal of Per- and Polyfluoroalkyl Substances (PFASs) in a Full-Scale Drinking Water Treatment Plant: Long-Term Performance of Granular Activated Carbon (GAC) and Influence of Flow-Rate. *Water Res.* **2020**, *182*, 115913.
(59) De Gooijer, J. M.; Ellmann, J.; Möller, M.; Koning, C. E. End Group Modification of Polyamide-6 in Supercritical and Subcritical Fluids: Part 3: Amine End Group Modification with Diketene and Diketene Acetone Adduct in CO2. *J. Supercrit. Fluids* **2004**, *31* (1), 75−87.
(60) Waltz, J. E.; Taylor, G. B. Determination of Molecular Weight of Nylon. *ACS Anal. Chem.* **1947**, *19* (7), 448−450.
(61) Mengerink, Y.; Peters, R.; Van Der Wal, S.; Claessens, H. A.; Cramers, C. A. Endgroup-Based Separation and Quantitation of Polyamide-6,6 by Means of Critical Chromatography. *J. Chromatogr. A* **2002**, *949*, 337−349.
(62) Brette, M. M.; Holm, A. H.; Drozdov, A. D.; Christiansen, J. d. C. Pure Hydrolysis of Polyamides: A Comparative Study. *Chemistry* **2024**, *6* (1), 13−50.
(63) Tang, C. Y.; Shiang Fu, Q.; Gao, D.; Criddle, C. S.; Leckie, J. O. Effect of Solution Chemistry on the Adsorption of Perfluorooctane Sulfonate onto Mineral Surfaces. *Water Res.* **2010**, *44* (8), 2654−2662.
(64) Gagliano, E.; Sgroi, M.; Falciglia, P. P.; Vagliasindi, F. G. A.; Roccaro, P. Removal of Poly- and Perfluoroalkyl Substances (PFAS) from Water by Adsorption: Role of PFAS Chain Length, Effect of Organic Matter and Challenges in Adsorbent Regeneration. *Water Res.* **2020**, *171*, 115381.
(65) Yu, J.; Lv, L.; Lan, P.; Zhang, S.; Pan, B.; Zhang, W. Effect of Effluent Organic Matter on the Adsorption of Perfluorinated Compounds onto Activated Carbon. *J. Hazard. Mater.* **2012**, *225−226*, 99−106.

https://doi.org/10.1021/acsestengg.3c00515
ACS EST Engg. 2024, 4, 995−1006

(66) Jia, C.; You, C.; Pan, G. Effect of Temperature on the Sorption and Desorption of Perfluorooctane Sulfonate on Humic Acid. *J. Environ. Sci.* **2010**, *22* (3), 355−361.
(67) Kretzschmar, R.; Sticher, H.; Hesterberg, D. Effects of Adsorbed Humic Acid on Surface Charge and Flocculation of Kaolinite. *Soil Sci. Soc. Am. J.* **1997**, *61* (1), 101−108.
(68) Chen, H.; Zhang, C.; Yu, Y.; Han, J. Sorption of Perfluorooctane Sulfonate (PFOS) on Marine Sediments. *Mar. Pollut. Bull.* **2012**, *64* (5), 902−906.
(69) Tasaki, T.; Oshima, T.; Baba, Y. Extraction Equilibrium and Membrane Transport of Copper (II) with New N-6-(t-Dodecylamido)-2-Pyridinecarboxylic Acid in Polymer Inclusion Membrane. *Ind. Eng. Chem. Res.* **2007**, *46* (17), 5715−5722.
(70) Deng, H.; Gao, L.; Zhang, S.; Yuan, J. Preparation of a Copper Ion Selective Membrane by Surface- Modified Molecular Imprinting. *Ind. Eng. Chem. Res.* **2012**, *51* (43), 14018−14025.
(71) Liu, G. Q.; Dotzauer, D. M.; Bruening, M. L. Ion-Exchange Membranes Prepared Using Layer-by-Layer Polyelectrolyte Deposition. *J. Membr. Sci.* **2010**, *354* (1−2), 198−205.
(72) Wijeratne, S.; Bruening, M. L.; Baker, G. L. Layer-by-Layer Assembly of Thick, Cu2+-Chelating Films. *Langmuir* **2013**, *29* (41), 12720−12729.
(73) Jiang, Y.; Wang, W. C. Functional Membranes Prepared by Layer-by-Layer Assembly and Its Metal Ions Adsorption Property. *Polym. Adv. Technol.* **2011**, *22* (12), 2509−2516.
(74) Magnenet, C.; Jurin, F. E.; Lakard, S.; Buron, C. C.; Lakard, B. Polyelectrolyte Modification of Ultrafiltration Membrane for Removal of Copper Ions. *Colloids Surf., A* **2013**, *435*, 170−177.
(75) Gao, B. J.; An, F. Q.; Zhu, Y. Novel Surface Ionic Imprinting Materials Prepared via Couple Grafting of Polymer and Ionic Imprinting on Surfaces of Silica Gel Particles. *Polymer* **2007**, *48* (8), 2288−2297.
(76) Zhang, F.; Wang, B.; He, S. F.; Man, R. L. Preparation of Graphene-Oxide/Polyamidoamine Dendrimers and Their Adsorption Properties toward Some Heavy Metal Ions. *J. Chem. Eng. Data* **2014**, *59* (5), 1719−1726.
(77) Chenette, H. C. S.; Robinson, J. R.; Hobley, E.; Husson, S. M. Development of High-Productivity, Strong Cation-Exchange Adsorbers for Protein Capture by Graft Polymerization from Membranes with Different Pore Sizes. *J. Membr. Sci.* **2012**, *423*−*424*, 43−52.
(78) Himstedt, H. H.; Qian, X. H.; Weaver, J. R.; Wickramasinghe, S. R. Responsive Membranes for Hydrophobic Interaction Chromatography. *J. Membr. Sci.* **2013**, *447*, 335−344.
(79) Chen, J. L.; Peng, R.; Chen, X. N. Hydrophobic Interaction Membrane Chromatography for Bioseparation and Responsive Polymer Ligands Involved. *Front. Mater. Sci.* **2017**, *11* (3), 197−214.
(80) Ma, A.; Hadi, P.; Barford, J.; Hui, C. W.; McKay, G. Modified Empty Bed Residence Time Model for Copper Removal. *Ind. Eng. Chem. Res.* **2014**, *53* (35), 13773−13781.
(81) Dragan, E. S.; Apopei Loghin, D. F.; Cocarta, A. I. Efficient Sorption of Cu2+ by Composite Chelating Sorbents Based on Potato Starch-Graft-Polyamidoxime Embedded in Chitosan Beads. *ACS Appl. Mater. Interfaces* **2014**, *6* (19), 16577−16592.
(82) Ouimet, J. A.; Xu, J.; Flores-Hansen, C.; Phillip, W. A.; Boudouris, B. W. Design Considerations for Next-Generation Polymer Sorbents: From Polymer Chemistry to Device Configurations. *Macromol. Chem. Phys.* **2022**, *223* (16), 2200032.
(83) Weidman, J. L.; Mulvenna, R. A.; Boudouris, B. W.; Phillip, W. A. Nanostructured Membranes from Triblock Polymer Precursors as High Capacity Copper Adsorbents. *Langmuir* **2015**, *31* (40), 11113−11123.
(84) Xu, J.; Slykas, C.; Braegelman, A. S.; Alvarez, K. G.; Kasl, T.; Boudouris, B. W.; Webber, M. J.; Sharma, V.; Phillip, W. A. Heavy Metal Removal Using Structured Sorbents 3D Printed from Carbon Nanotube-Enriched Polymer Solutions. *Matter* **2022**, *5* (10), 3432−3451.
(85) Ochoa-Herrera, V.; Sierra-Alvarez, R. Removal of Perfluorinated Surfactants by Sorption onto Granular Activated Carbon, Zeolite and Sludge. *Chemosphere* **2008**, *72* (10), 1588−1593.

https://doi.org/10.1021/acsestengg.3c00515
ACS EST Engg. 2024, 4, 995−1006